Published in final edited form as:
Mult Scler. 2014 October ; 20(11): 1464–1470. doi:10.1177/1352458514525868.

Rapid, high-resolution, whole-brain, susceptibility-based MRI of multiple sclerosis

P. Sati[1], **D. M. Thomasson**[2], **N. Li**[3], **D. L. Pham**[3], **N. M. Biassou**[4], **D. S. Reich**[1,4,*], and **J. A. Butman**[4,*]

[1] Translational Neuroradiology Unit, Neuroimmunology Branch, National Institute of Neurological Disorders and Stroke, National Institutes of Health, Bethesda, Maryland, USA

[2] Integrated Research Facility, National Institute of Allergy and Infectious Diseases, National Institutes of Health, Bethesda, Maryland, USA

[3]Image Processing Core, Center for Neuroscience and Regenerative Medicine, National Institutes of Health, Bethesda, Maryland, USA

[4] Radiology and Imaging Sciences, Department of Diagnostic Radiology, Clinical Center, National Institutes of Health, Bethesda, Maryland, USA

Abstract

Background and Purpose: Susceptibility-based MRI offers a unique opportunity to study neurological diseases such as multiple sclerosis (MS). In this work, we assessed a three-dimensional segmented echo-planar-imaging (3D-EPI) sequence to rapidly acquire high-resolution T_2^*-weighted and phase contrast images of the whole brain. We also assessed if these images could depict important features of MS at clinical field strength, and we tested the effect of a gadolinium-based contrast agent (GBCA) on these images.

Materials and Methods: The 3D-EPI acquisition was performed on four healthy volunteers and fifteen MS cases on a 3T scanner. The 3D sagittal images of the whole brain were acquired with a voxel size of $0.55 \times 0.55 \times 0.55$ mm^3 in less than 4 minutes. For the MS cases, the 3D-EPI acquisition was performed before, during, and after intravenous GBCA injection.

Results: Both T_2^*-weighted and phase-contrast images from the 3D-EPI acquisition were sensitive to the presence of lesions, parenchymal veins, and tissue iron. Conspicuity of the veins was enhanced when images were obtained during injection of GBCA.

Conclusions: We propose this rapid imaging sequence for investigating, in a clinical setting, the spatiotemporal relationship between small parenchymal veins, iron deposition, and lesions in MS patient brains.

Keywords

Multiple sclerosis; brain imaging; MRI; contrast agent; lesion; veins; iron

Corresponding author: Dr. Pascal Sati Translational Neuroradiology Unit, National Institute of Neurological Disorders and Stroke National Institutes of Health 9000 Rockville Pike Building 10/5C101A Bethesda, MD 20892-1584 Phone#: 301-402-1436 Fax#: 301-402-0373 satip@ninds.nih.gov.
*These authors contributed equally.

Introduction

Susceptibility-based MRI contrast (referring both to contrast generated by T_2^* signal loss and phase accumulation from non-refocused gradient echoes) enables the study of fine anatomical details within gray and white matter (1). Susceptibility contrast is also extremely useful to study neuronal activation (2), image parenchymal veins (3), and detect hemorrhage (4) or calcification (5). In addition, T_2^*can be used to gauge tissue iron (6) and could potentially assess myelin content (7). Therefore, susceptibility-based imaging is an attractive MRI tool for characterizing in vivo brain tissue changes caused by neurological diseases. This is of particular interest in MS, where it has been already applied at various field strengths to characterize veins inside WM lesions (8, 9), cortical lesions (10, 11), iron-laden macrophages at the edge of certain lesions (10, 12), iron deposition inside deep gray nuclei (13, 14), and the severity of parenchymal tissue destruction (15).

However, in most of these studies T_2^* imaging was performed using a conventional spoiled (2D or 3D) gradient echo (GRE) sequence, which requires a compromise between high isotropic resolution and whole-brain coverage to avoid excessively long scan times. As a result, high resolution imaging is typically limited to the supratentorial brain, thus neglecting the brainstem and cerebellum, both of which are often severely affected in MS (16, 17). If whole brain coverage is desired , the use of small isotropic voxel dimensions (< 1 mm^3 in volume) is usually avoided; high-resolution is achieved in one plane only (typically the axial plane), whereas resolution in the slice direction remains relatively low (usually 2 to 4 mm). Such anisotropic voxels render fine anatomical details related to the disease difficult to visualize in 3 planes, and these details can even be missed due to the partial volume effect caused by the use of large slice thicknesses. More broadly, these limitations hamper the optimal use of susceptibility imaging in a clinical environment, where acquisition speed and whole-brain coverage are required.

Recently, a different acquisition strategy has been introduced at ultra-high field, allowing fast, high-resolution susceptibility imaging of the whole brain (18). In a manner analogous to using an echo train to accelerate spin echo sequences (so-called fast or turbo spin echo), a three-dimensional segmented echo-planar-imaging (3D-EPI) sequence can be used to accelerate GRE imaging. Using such 3D-EPI in healthy brains at 7T, T_2^*-weighted and phase contrast with high anatomic fidelity, and a considerable gain in volume coverage relative to conventional GRE images, were obtained without sacrificing scan time (18). Therefore, in this work, we investigated whether 3D-EPI is feasible at clinical field strength (3T) and can provide useful T_2^*-weighted and phase contrast in the evaluation of MS. Because the relationship of MS plaques to parenchymal veins is an active area of research (19, 20), we also tested the effect of gadolinium-based contrast agent (GBCA) on the conspicuity of veins in 3D-EPI images obtained before, during, and after the injection of contrast agent.

Materials and Methods

Imaging was performed on 4 healthy participants (4 men, age 37±6 years) and 15 MS cases (10 men, 5 women, age 43±13 years), all of whom gave written, informed consent to participate in an Institutional Review Board-approved protocol. 3D-EPI was acquired using a 3T MRI system (Philips Healthcare, Best, The Netherlands) with the manufacturer's eight-channel receive-only head coil and body transmit coil. An automated whole-brain first-order shimming procedure provided by the manufacturer was performed before acquisition. The 3D-EPI acquisition used 0.55×0.55×0.55 mm^3 voxels (0.17 mm^3 voxel volume) covering the whole brain (336 slices). This acquisition relied on the manufacturer's segmented EPI readout using a Cartesian interleaved k-space trajectory and an EPI factor of 15 lines per excitation. Acquisition was three-dimensional (3D) and performed in the sagittal plane with a parallel imaging (Sensitivity Encoding for Fast MRI, also called SENSE) factor of 2 in both left-right (i.e. slice-encoding) and anterior-posterior (i.e. phase-encoding) directions. A fat suppression prepulse removed the artifacts resulting from shifted fat signal (water–fat shift of 9.6 mm here).This was achieved using a fat-selective binomial spatial and spectral saturation pulse from the manufacturer ("Proset 1331"). Other parameters were: field of view = 220 (anterior-posterior) × 220 (foot-head) × 185 (left-right) mm^3, flip angle = 10 °, repetition time = 54 ms, echo time = 29 ms, number of slices = 336, bandwidth in the readout direction = 490 Hz/pixel, bandwidth in the phase-encoding direction = 27 Hz/pixel. For improved signal-to-noise ratio (SNR), the sequence was acquired twice (number of excitations = 2), giving a total scan time under 4 min.

To test the effect of GBCA on venous contrast, the 3D-EPI acquisition was repeated for all 15 MS cases at three different times during the scanning: before, during and, approximately 15 min after GBCA injection. The GBCA was a single dose of gadopentetate dimeglumine (Magnevist; Bayer Healthcare, Leverkusen, Germany) or gadobutrol (Gadavist; Bayer Healthcare, Leverkusen, Germany) injected intravenously over 60 seconds. The infusion of GBCA was started simultaneously with the second 3D-EPI acquisition using a power injector (MEDRAD, Warrendale, PA).

Magnitude and phase images were collected as DICOM data produced by the MRI scanner. All analyses done on the magnitude images were performed using Matlab (The MathWorks, Natick, MA) and MIPAV (Medical Image Processing, Analysis & Visualization, NIH). For the phase images, an automatic analytical phase unwrapping was employed as described in (21). Following phase unwrapping, large background gradients were removed by performing Gaussian filtering with a filter size of 32 pixels and full width at half maximum of 8 pixels (22).

To measure the SNR of the magnitude 3D-EPI images, two consecutive acquisitions were performed on the 4 healthy participants. Using the dual-acquisition subtraction method (23) , the SNR was calculated as:

(1)

where SI_1 is the mean intensity in the region-of-interest (ROI) on the first magnitude image, and $SD_{1\text{-}2}$ is the standard deviation in the ROI on the subtraction magnitude image. A transverse slice passing though the genu and splenium of the corpus callosum of the healthy subjects was selected and, a 160×160 pixel ROI centered inside the brain parenchyma was used for calculating the SNR.

To measure contrast-to-noise ratio (CNR) between two different types of brain tissue, the mean intensities of the two tissues of interest (SI_1 for tissue 1 and SI_2 for tissue 2) were used as input in the following equation:

(2)

For the $CNR_{lesion\text{-}WM}$, ROIs were drawn manually for the lesions detected on a transverse slice passing though the genu and splenium of the corpus callosum. A nearby ROI with normal appearing white matter was also drawn on this slice. For $CNR_{GP\text{-}WM}$ and $CNR_{DN\text{-}WM}$, ROIs were drawn on a sagittal slice where both the globus pallidus (GP) and the dentate nucleus (DN) were visible. A region of normal appearing deep white matter was also drawn on this slice. For the $CNR_{vein\text{-}WM}$, a minimum intensity projection (mIP) was first performed across 15 slices (i.e. 7.5 mm) along the head-foot direction at the level of the corpus callosum for the before, during- and after injection acquisitions. A mIP image of the pre-injection acquisition revealing the deep medullary veins of the white matter (WM) was selected, onto which a ROI primarily containing small veins was drawn. A nearby ROI without any apparent blood vessels was also drawn on the same mIP image. To quantify the effect of GBCA on the conspicuity of small parenchymal veins, the same ROIs were applied to them IP images of the during and after injection acquisitions. All the CNR calculations were performed across the 15 MS cases. Mean values and standard deviation values across the 15 cases are mentioned in the Results section.

A count of the lesions with and without a central vein was also performed for the 15 MS cases using the same transverse slice as the one previously selected for $CNR_{lesion\text{-}WM}$ calculations. Finally, lesions with a hypointense rim on magnitude image were counted when examining all the brain slices of the 15 MS patients.

Results

3D-EPI measurements performed in healthy volunteers yielded an SNR of 9.4 ± 1.0 (mean ± standard deviation across n = 4 volunteers). In MS cases, the 3D-EPI T_2^*-weighted images displayed WM lesions (red arrows in Fig 1) as hyperintensities ($CNR_{lesion\text{-}WM}$= 0.14 ± 0.04). In our MS cohort, only one patient showed hyperintense lesions with a hypointense rim (n=3 lesions), most likely attributed to iron-loaded macrophages (10). Parenchymal

veins appeared as hypointense structures ($CNR_{vein\text{-}WM} = -0.09 \pm 0.05$) with a round or linear shape, depending on their orientation relative to the visualization plane. Some of the deep gray matter nuclei, particularly globus pallidus and dentate nucleus (green arrows in Fig 1), also appeared hypointense ($CNR_{GP\text{-}WM} = -0.16 \pm 0.07$ and $CNR_{DN\text{-}WM} = -0.17 \pm 0.11$). As expected for a gradient-echo based acquisition, 3D-EPI images also suffered from some signal losses in brain areas close to air/tissue interfaces, especially the paranasal sinuses and mastoid air cells (blue arrows in Fig 1).

Phase contrast images derived from the 3D-EPI acquisition provided complementary information about the disease (Fig 2). Some lesions detected on T_2^*-weighted images appeared hypointense on the phase contrast (more paramagnetic relative to WM; Fig 2B), whereas others appeared isointense to WM with a hypointense rim (paramagnetic rim; Fig 2A).

The effect of GBCA injection on the conspicuity of small veins is shown in Fig 3. Comparison of the before, during, and after GBCA mIP images demonstrates that the conspicuity of the small deep medullary veins was maximal when the 3D-EPI acquisition occurred during injection ($CNR_{vein\text{-}WM} = -0.19 \pm 0.07$, mean ± standard deviation, n=4 healthy volunteers) as compared with the acquisition before ($CNR_{vein\text{-}WM} = -0.09 \pm 0.05$) and ~15 min after injection ($CNR_{vein\text{-}WM} = -0.10 \pm 0.05$). Note that the use of GBCA allowed for clear delineation of central veins within lesions, which were poorly visible prior to contrast injection. These central veins were detected inside many WM lesions, especially in the periventricular and deep WM areas (Fig 4). In those WM areas, up to 96% of the lesions (123 out of 128 lesions) detected in our MS cohort depicted a central vein. Note that this colocalization of veins and MS lesions could also be observed in the cerebellum (Fig 5).

Discussion

This study describes the use of a fast 3D segmented EPI acquisition that provides whole-brain, high-resolution (voxel size of $0.55 \times 0.55 \times 0.55$ mm^3) T_2^*-weighted and phase images at 3T in less than 4 min. This acquisition was developed for routine clinical scanning using the manufacturer's 3D-EPI sequence and standard phased-array receiver (eight-channel head coil).

From a technical standpoint, the use of a 3D-EPI sequence, instead of the more conventional GRE, offers substantial advantages. As recently demonstrated (18), the 3D segmented EPI acquisition allows faster acquisition speeds, greater brain coverage, and higher SNR than standard GRE. Moreover, the use of high isotropic resolution with the 3D-EPI acquisition enables the visualization of fine anatomical details as well as the reformatting of images in any plane. Although this is an EPI-based acquisition, we did not notice significant distortions in most of the brain, most likely due to the segmented readout. Only a slight distortion (maximum ~4-5 mm) was observed at some of the brain edges.

From a clinical perspective, this 3D-EPI acquisition could be used to study in vivo the relationship between WM lesions and parenchymal vasculature, since it can depict both features on the same image. Such study could assess the role of parenchymal veins in the

pathogenesis of MS lesions, which might act as a conduit for the inflammatory cells (24) that trigger their development and growth (25). Note that to further improve the detection of both veins and WM lesions on the same image, one could also combine our 3D EPI acquisition with a 3D FLAIR to produce the so-called FLAIR* contrast (26, 27).

The first MRI report of colocalization of MS lesions and veins was published by Tan and colleagues in 2000 and used a conventional GRE acquisition at low field strength (1.5T)(8). Since then, several studies have reproduced that finding while optimizing the imaging protocols for use at higher field strengths (3T and 7T) (19, 28, 29). Based on these reports, it has been suggested that the diagnostic criteria for MS might be refined by including the detection, by MRI, of a central vein inside lesions (20). Whether detection of such veins will increase diagnostic accuracy for MS still awaits further investigation (30), but the 3D-EPI technique could be used to address this question. Indeed, as demonstrated here, the 3D-EPI acquisition can be performed on a 3T MRI platform operating in a clinical environment, thus making it appropriate for large-scale, longitudinal studies of patients with various neurological conditions mimicking the MRI presentation of MS.

Another important clinical feature of the 3D-EPI acquisition concerns its extreme sensitivity to non-heme iron present in the brain parenchyma. Indeed, both T_2^*-weighted and phase contrast EPI are able to detect lesions with a hypointense rim. Initially reported at 7T (31), this type of lesion has been recently characterized ex vivo by combining MRI and histology (10), and its hypointense rim has been attributed to iron-laden macrophages and microglia. Longitudinal observations with the 3E EPI technique could help to further understand differences in the pathogenesis of this type of lesion in comparison to other MS lesions. As illustrated here for the globus pallidus and dentate nucleus, 3D-EPI images can also be used to track brain areas (including putamen, caudate nucleus, and thalamus) known to experience non-heme iron deposition, which may be accentuated in MS (13). However, a current limitation of our 3D-EPI protocol is that it allows data acquisition at only one echo time, meaning that the presence of iron cannot be evaluated quantitatively from magnitude images via T_2^* relaxation-time mapping (13). A solution would be to use instead quantitative susceptibility mapping (QSM), which has recently emerged as a method to identify and quantify iron deposition in deep gray nuclei of MS brains (33). Since the calculation of these susceptibility maps relies on solving an inverse problem from gradient-echo phase data, it can in principle be applied to the 3D-EPI phase images in a straight forward manner.

Conclusions

This study describes the use of a rapid, ultra-high-resolution (isotropic voxels of 0.17 mm^3 volume) imaging protocol in MS patients on a clinical 3T scanner using a manufacturer-provided pulse sequence. Whole-brain coverage was achieved in less than 4 min, yielding T_2^*-weighted and phase images via a 3D segmented EPI acquisition. These images are sensitive to MS lesions as well as to parenchymal veins and tissue iron. We tested the effect of gadolinium-based contrast agent by performing the acquisition during the injection of contrast and found that it further enhances the detection of small parenchymal veins. Thus, we propose to use this approach for investigating, on a large scale, the spatiotemporal

relationship between parenchymal veins and lesions, as well as the development of lesions with a rim of iron-laden macrophages and the deposition of tissue iron in deep gray matter, that can occur in the brains of people with MS.

Acknowledgments

The authors acknowledge the Intramural Research Program of the National Institute of Neurological Disorders and Stroke and the NIH Clinical Center Radiology technologists for their work in acquiring the data, the Neuroimmunology Branch clinical group for coordinating recruitment and evaluation of patients, Dr John Ostuni from the NINDS image processing facility, and Dr Joseph Frank for access to a research imager for initial development of the technique.

References

1. Duyn JH. Study of brain anatomy with high-field MRI: recent progress. Magn Reson Imaging. 2010; 28:1210–1215. [PubMed: 20392587]
2. Ogawa S, Lee TM, Kay AR, Tank DW. Brain magnetic resonance imaging with contrast dependent on blood oxygenation. Proc Natl Acad Sci U S A. 1990; 87:9868–9872. [PubMed: 2124706]
3. Reichenbach JR, Venkatesan R, Schillinger DJ, Kido DK, Haacke EM. Small vessels in the human brain: MR venography with deoxyhemoglobin as an intrinsic contrast agent. Radiology. 1997; 204:272–277. [PubMed: 9205259]
4. Scharf J, Brauherr E, Forsting M, Sartor K. Significance of haemorrhagic lacunes on MRI in patients with hypertensive cerebrovascular disease and intracerebral haemorrhage. Neuroradiology. 1994; 36:504–508. [PubMed: 7845571]
5. Wu Z, Mittal S, Kish K, Yu Y, Hu J, Haacke EM. Identification of calcification with MRI using susceptibility-weighted imaging: a case study. J Magn Reson Imaging. 2009; 29:177–182. [PubMed: 19097156]
6. Haacke EM, Cheng NY, House MJ, et al. Imaging iron stores in the brain using magnetic resonance imaging. Magn Reson Imaging. 2005; 23:1–25. [PubMed: 15733784]
7. Hwang D, Kim DH, Du YP. In vivo multi-slice mapping of myelin water content using T2* decay. Neuroimage. 2010; 52:198–204. [PubMed: 20398770]
8. Tan IL, van Schijndel RA, Pouwels PJ, et al. MR venography of multiple sclerosis. AJNR Am J Neuroradiol. 2000; 21:1039–1042. [PubMed: 10871010]
9. Ge Y, Zohrabian VM, Osa EO, et al. Diminished visibility of cerebral venous vasculature in multiple sclerosis by susceptibility-weighted imaging at 3.0 Tesla. J Magn Reson Imaging. 2009; 29:1190–1194. [PubMed: 19388109]
10. Pitt D, Boster A, Pei W, et al. Imaging cortical lesions in multiple sclerosis with ultra-high-field magnetic resonance imaging. Arch Neurol. 2010; 67:812–818. [PubMed: 20625086]
11. Cohen-Adad J, Benner T, Greve D, et al. In vivo evidence of disseminated subpial T2* signal changes in multiple sclerosis at 7 T: a surface-based analysis. Neuroimage. 2011; 57:55–62. [PubMed: 21511042]
12. Hammond KE, Metcalf M, Carvajal L, et al. Quantitative in vivo magnetic resonance imaging of multiple sclerosis at 7 Tesla with sensitivity to iron. Ann Neurol. 2008; 64:707–713. [PubMed: 19107998]
13. Khalil M, Enzinger C, Langkammer C, et al. Quantitative assessment of brain iron by R(2)* relaxometry in patients with clinically isolated syndrome and relapsing-remitting multiple sclerosis. Mult Scler. 2009; 15:1048–1054. [PubMed: 19556316]
14. Haacke EM, Makki M, Ge Y, et al. Characterizing iron deposition in multiple sclerosis lesions using susceptibility weighted imaging. J Magn Reson Imaging. 2009; 29:537–544. [PubMed: 19243035]
15. Sati P, Cross AH, Luo J, Hildebolt CF, Yablonskiy DA. In vivo quantitative evaluation of brain tissue damage in multiple sclerosis using gradient echo plural contrast imaging technique. Neuroimage. 2010; 51:1089–1097. [PubMed: 20338247]

16. Barnett MH, Prineas JW. Relapsing and remitting multiple sclerosis: pathology of the newly forming lesion. Ann Neurol. 2004; 55:458–468. [PubMed: 15048884]

17. Kutzelnigg A, Faber-Rod JC, Bauer J, et al. Widespread demyelination in the cerebellar cortex in multiple sclerosis. Brain Pathol. 2007; 17:38–44. [PubMed: 17493036]

18. Zwanenburg JJ, Versluis MJ, Luijten PR, Petridou N. Fast high resolution whole brain T2* weighted imaging using echo planar imaging at 7T. Neuroimage. 2011; 56:1902–1907. [PubMed: 21440070]

19. Tallantyre EC, Brookes MJ, Dixon JE, Morgan PS, Evangelou N, Morris PG. Demonstrating the perivascular distribution of MS lesions in vivo with 7-Tesla MRI. Neurology. 2008; 70:2076–2078. [PubMed: 18505982]

20. Mistry N, Dixon J, Tallantyre E, et al. Central veins in brain lesions visualized with high-field magnetic resonance imaging: a pathologically specific diagnostic biomarker for inflammatory demyelination in the brain. JAMA Neurol. 2013; 70:623–628. [PubMed: 23529352]

21. Schofield MA, Zhu Y. Fast phase unwrapping algorithm for interferometric applications. Optics Letters. 2003; 28:1194–1196. [PubMed: 12885018]

22. Li, N.; Wang, WT.; Sati, P.; Pham, DL.; Butman, JA. SPIE Medical Imaging. San Diego, CA: 2012. Quantitative evaluation of phase processing approaches in susceptibility weighted imaging.

23. Price RR, Axel L, Morgan T, et al. Quality assurance methods and phantoms for magnetic resonance imaging: report of AAPM nuclear magnetic resonance Task Group No. 1. Med Phys. 1990; 17:287–295. [PubMed: 2333055]

24. Lucchinetti C, Bruck W, Parisi J, Scheithauer B, Rodriguez M, Lassmann H. Heterogeneity of multiple sclerosis lesions: implications for the pathogenesis of demyelination. Ann Neurol. 2000; 47:707–717. [PubMed: 10852536]

25. Gaitan MI, Shea CD, Evangelou IE, et al. Evolution of the blood-brain barrier in newly forming multiple sclerosis lesions. Ann Neurol. 2011; 70:22–29. [PubMed: 21710622]

26. Sati P, George IC, Shea CD, Gaitan MI, Reich DS. FLAIR*: a combined MR contrast technique for visualizing white matter lesions and parenchymal veins. Radiology. 2012; 265:926–932. [PubMed: 23074257]

27. Kilsdonk ID, Wattjes MP, Lopez-Soriano A, et al. Improved differentiation between MS and vascular brain lesions using FLAIR* at 7 Tesla. Eur Radiol. 2013

28. Tallantyre EC, Morgan PS, Dixon JE, et al. A comparison of 3T and 7T in the detection of small parenchymal veins within MS lesions. Invest Radiol. 2009; 44:491–494. [PubMed: 19652606]

29. Tallantyre EC, Dixon JE, Donaldson I, et al. Ultra-high-field imaging distinguishes MS lesions from asymptomatic white matter lesions. Neurology. 2011; 76:534–539. [PubMed: 21300968]

30. Quinn MP, Kremenchutzky M, Menon RS. Venocentric Lesions: An MRI Marker of MS? Front Neurol. 2013; 4:98. [PubMed: 23885252]

31. Kollia K, Maderwald S, Putzki N, et al. First clinical study on ultra-high-field MR imaging in patients with multiple sclerosis: comparison of 1.5T and 7T. AJNR Am J Neuroradiol. 2009; 30:699–702. [PubMed: 19147714]

32. Lassmann H. The pathologic substrate of magnetic resonance alterations in multiple sclerosis. Neuroimaging Clin N Am. 2008; 18:563–576. [PubMed: 19068402]

33. Langkammer C, Liu T, Khalil M, et al. Quantitative susceptibility mapping in multiple sclerosis. Radiology. 2013; 267:551–559. [PubMed: 23315661]

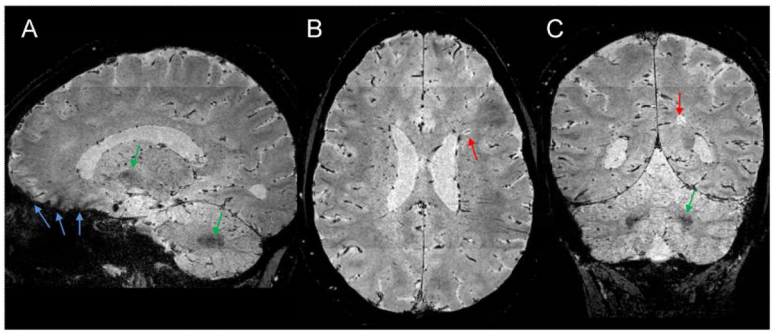

Figure 1.

3D-EPI magnitude images from one MS case acquired at 3T using a voxel resolution of 0.55 × 0.55 × 0.55 mm^3. 3D-EPI images are initially acquired in the sagittal plane (A) and then reformatted in the axial (B) and coronal (C) planes. Red arrows point to MS lesions in the white matter. Green arrows indicate thalamus and dentate nucleus. Blue arrows show areas of signal loss close to air/tissue interfaces (paranasal sinuses and mastoid air cells).

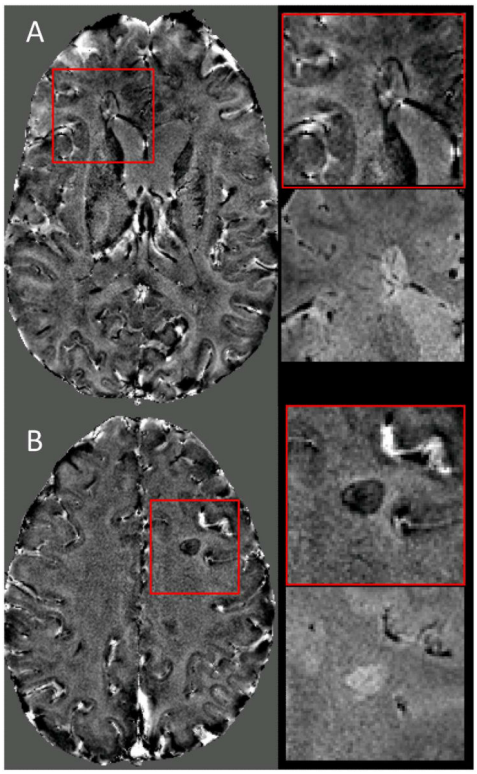

Figure 2.

3D-EPI phase images from two different MS cases (A & B) scanned at 3T. Magnified boxes show two lesions detected on phase contrast images (red boxes) and their corresponding T_2^*-weighted images from the same acquisition.

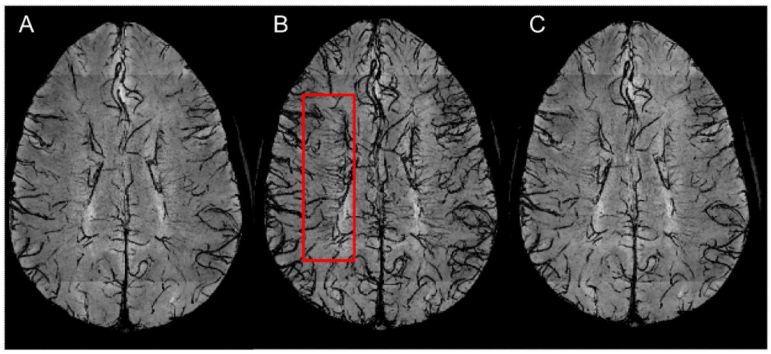

Figure 3.

3D-EPI minimum intensity projection (mIP) magnitude images from an MS case acquired before (A), during (B), and 15 min after (C) the injection of GBCA. The mIP was performed across 15 slices (i.e. 7.5 mm) along the head-foot direction at the level of the corpus callosum, in order to show the deep medullary veins of the WM (red box).

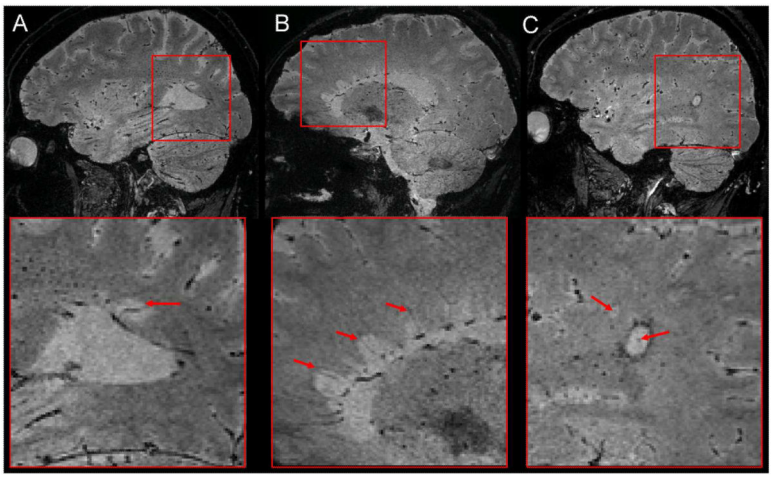

Figure 4.

3D-EPI magnitude images from three different MS cases (A, B, and C) acquired during contrast agent injection. The colocalization of the veins and periventricular MS lesions (“Dawson's fingers”) can be easily detected in the first two cases (red arrows inside magnified boxes of A and B).The third case also shows two lesions with a central vein (red arrows inside magnified boxes of C), but one lesion (the largest one) also displays a hypointense rim at its edge.

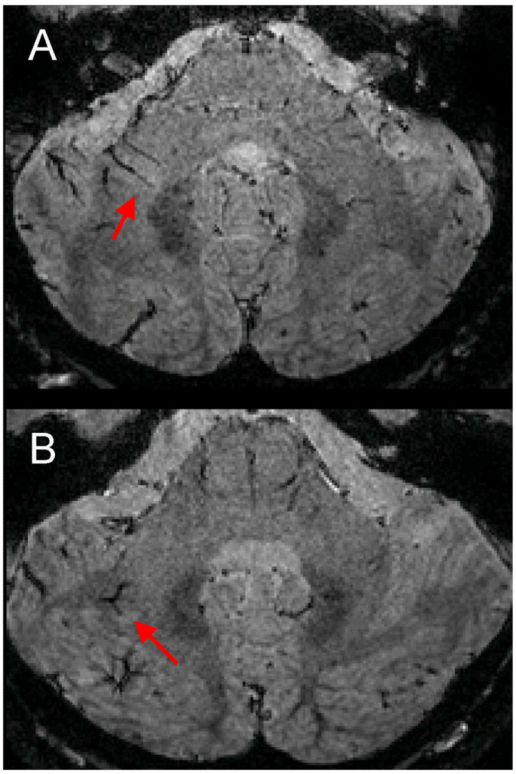

Figure 5.
3D-EPI magnitude images from the cerebellum of two different MS cases (A & B). Red arrows point to hyperintense lesions with a vein running through them.